



**POLITECNICO**  
MILANO 1863

**[RE.PUBLIC@POLIMI](mailto:RE.PUBLIC@POLIMI)**

Research Publications at Politecnico di Milano

## Post-Print

This is the accepted version of:

P. Bortolotti, C.L. Bottasso, A. Croce, L. Sartori  
*Integration of Multiple Passive Load Mitigation Technologies by Automated Design Optimization - the Case Study of a Medium-Size Onshore Wind Turbine*  
Wind Energy, Vol. 22, N. 1, 2019, p. 65-79  
doi:10.1002/we.2270

The final publication is available at <https://doi.org/10.1002/we.2270>

Access to the published version may require subscription.

This is the peer reviewed version of the following article: Integration of Multiple Passive Load Mitigation Technologies by Automated Design Optimization - the Case Study of a Medium-Size Onshore Wind Turbine, which has been published in final form at <https://doi.org/10.1002/we.2270>. This article may be used for non-commercial purposes in accordance with Wiley Terms and Conditions for Use of Self-Archived Versions.

**When citing this work, cite the original published paper.**

Permanent link to this version

<http://hdl.handle.net/11311/1073942>

RESEARCH ARTICLE

# Integrated Design Studies of a Multi-MW Onshore Wind Turbine

Pietro Bortolotti<sup>1</sup>, Luca Sartori<sup>2</sup>, Alessandro Croce<sup>2</sup>, and Carlo L. Bottasso<sup>1,2</sup>

<sup>1</sup>Wind Energy Institute, Technische Universität München, D-85748 Garching b. München, Germany

<sup>2</sup>Dipartimento di Scienze e Tecnologie Aerospaziali, Politecnico di Milano, I-20156 Milano, Italy

## ABSTRACT

Continuous efforts are being dedicated to the improvement of wind energy systems, ultimately aiming at the minimization of cost of energy. Systems engineering design methodologies can assist wind turbine designers in this challenge by developing different design configurations and by evaluating them from a holistic perspective. This paper applies the latest advancements in these methodologies to conduct design studies on a wind turbine model representative of modern land-based machines. A reference design is first developed and later adopted to benchmark several load-alleviating blade configurations adopting swept shapes, composite fibers misalignment and geometrical solutions such as spar caps and shear webs offsets. In addition, a regulation trajectory that reduces the energy loss generated by bend-twist coupled rotor is proposed. Finally, a load-alleviating wind turbine configuration is investigated combining sweep and composite fibers misalignment. The final design generates cost of energy savings of 2.8% thanks to a highly coned - soft - larger rotor that results in lower turbine costs and a higher energy capture compared to the baseline design. Copyright © 2018 John Wiley & Sons, Ltd.

## KEYWORDS

Systems Engineering, Wind Turbine Design, Onshore Wind

## Correspondence

Wind Energy Institute, Technische Universität München, D-85748 Garching b. München.

E-mail: carlo.bottasso@tum.de

Received . . .

## 1. INTRODUCTION

The design of a wind turbine is a complex optimization process, which has to account for the tight interactions existing among multiple disciplines and the presence of several concurrent and often contrasting design requirements. As in many aeronautic applications, the design of wind turbines must inherently be a trade-off between aerodynamics, structures and cost efficiency. Indeed, on the one hand an aerodynamically optimum wind turbine features a very low rotor solidity, high rotational speeds and very thin airfoil shapes. On the opposite, a structurally efficient design benefits from thick profiles, large chord distributions and low rotational speeds. In parallel to these two contrasting disciplines, the imperative goal of cost reduction narrows the solution space limiting the choice of, for example, manufacturing processes as well as materials. Finally, onshore machines must meet noise emission limits as well as transportability requirements. For such challenge, automated systems engineering tools can greatly simplify and speed-up the exploration of the design space, and can improve the understanding of the effects of design choices and trade-offs. The present work reports on some latest developments in the field of automated design optimization of wind turbines and their application to perform design studies of a multi-MW wind turbine representative of modern onshore machines.

Wind turbine manufacturers internally develop or externally purchase industrial tools for their systems engineering design activities. However, in the public domain only few comprehensive wind turbine modeling and design frameworks are described in detail. For a number of years our group has been involved in the development of one of them, the Code for Performance Maximization  $C_p$ -Max, whose implemented methodologies are described in several publications, such as Bottasso et al., 2011 [1], Bottasso et al., 2015 [2] and Bortolotti et al., 2016a [3]. Two other well known research frameworks are the open-access tools Wind-Plant Integrated System Design and Engineering Model WISDEM [4] and

the Multidisciplinary Horizontal Axis Wind Turbine Optimization Tool *HAWTOpt2* [5], which are developed by the National Renewable Energy Laboratory (NREL) in the U.S. and by Denmark Technical University (DTU) respectively. In addition, thanks to a growing interest in the area of wind turbine systems engineering more research institutes are currently dedicating efforts to the development of publicly available tools.

*C<sub>p</sub>-Max*, which is continuously upgraded and expanded, performs the overall sizing of a wind turbine in terms of rotor diameter and tower height, while simultaneously generating a detailed sizing of the aerodynamic and structural components of the machine, ultimately aiming at the minimization of the cost of energy (CoE). During the design process, the control laws governing the machine are updated automatically, as they play a central role in determining the performance and loading of a wind turbine. The design approach is based on multi-fidelity modeling of the system, where 2D cross sectional models, multibody-based aeroservoelastic models and full 3D FEM models are used at different stages of the overall process. The use of the various fidelity models is based on the need to balance accuracy with computational cost. The design methodology respects the certification guidelines prescribed by international standards [6].

The code has been recently upgraded with new modules to further enlarge the available solution space. Advancements include the possibility to model and optimize the prebend curvature of the blades [7], the possibility to model arbitrary blade sweep curvatures and lastly the possibility to treat composite materials as design variables [8]. This latest release of *C<sub>p</sub>-Max* is here exercised on the design optimization of a 3 MW class wind turbine, which has been developed within the framework of the IEA Wind Task 37 [9]. This wind turbine model is first developed for a given set of parameters and later used as starting point for an integrated design optimization, investigating the existence of alternative configurations that lead to a reduction of the CoE. Specifically, attention is focused on wind turbine configurations equipped with passive load alleviation methods. These include parametric studies on different sweep curvatures, composite fibers misalignment and changes in the blade internal geometry. The three technologies for load alleviation are first analyzed individually and later merged trying to join the pros while limiting the cons of each of them. This integration is also combined with the definition of a regulation trajectory aimed at minimizing the power losses originated by the load alleviating rotors. As last step of the work, an optimum wind turbine design is investigated for a load alleviating rotor configuration by running *C<sub>p</sub>-Max* in a completely automatic modality, exercising the full capabilities of the optimization algorithms.

The discussion is articulated as follows. After the introduction, Sect. 2 presents the simulations and design tools adopted in this study. Then, applications are reported in Sect. 3 with the development of the baseline configuration characterized by a traditional design and in Sect. 4 where several design studies on load alleviating technologies are reported. The conclusions of the study and the outlook on future work are reported in Sect. 5.

## 2. DESIGN AND SIMULATION TOOLS

*C<sub>p</sub>-Max* is a wind turbine simulation and design suit implemented in MATLAB® [10]. Wind turbine models are described by an Excel data worksheet and the following simulations can be readily performed:

- Computation of the natural frequencies of the system.
- Power-thrust-torque performance study.
- Computation and post-processing of extreme and fatigue loads.
- Aeroacoustic analysis through semi-empirical models.

In the optimization module of *C<sub>p</sub>-Max*, the code combines a detailed aerodynamic optimization module and a detailed structural optimization module within an outer optimization loop for the overall aero-structural optimization of the wind turbine. A detailed description of the algorithmic architecture of the tool is available in Bottasso et al., 2011 [1] and Bortolotti et al., 2016a [3]. A recall is here shortly elaborated and graphically depicted in Fig. 1. The merit figure, optimization variables and constraints of the design process are so structured.

### Design variables:

- Aerodynamic optimization - user-defined control points for chord and twist distributions, positions along blade span of pre-assumed airfoils.
- Structural optimization - thicknesses along blade span and composite selector of up to 15 structural components of the blade, diameters and thicknesses of an arbitrary number of truncated steel cones piled together modeling the turbine tower.
- Macro optimization - rotor diameter, hub height, nacelle up tilt angle, rotor cone angle, maximum allowable blade tip speed and in-plane and out-of-plane blade aero-shape parameters from Eq. 1.

### Merit figure:

- Aerodynamic optimization - maximization of the Annual Energy Production (AEP).
- Structural optimization - minimization of the Initial Capital Cost (ICC).

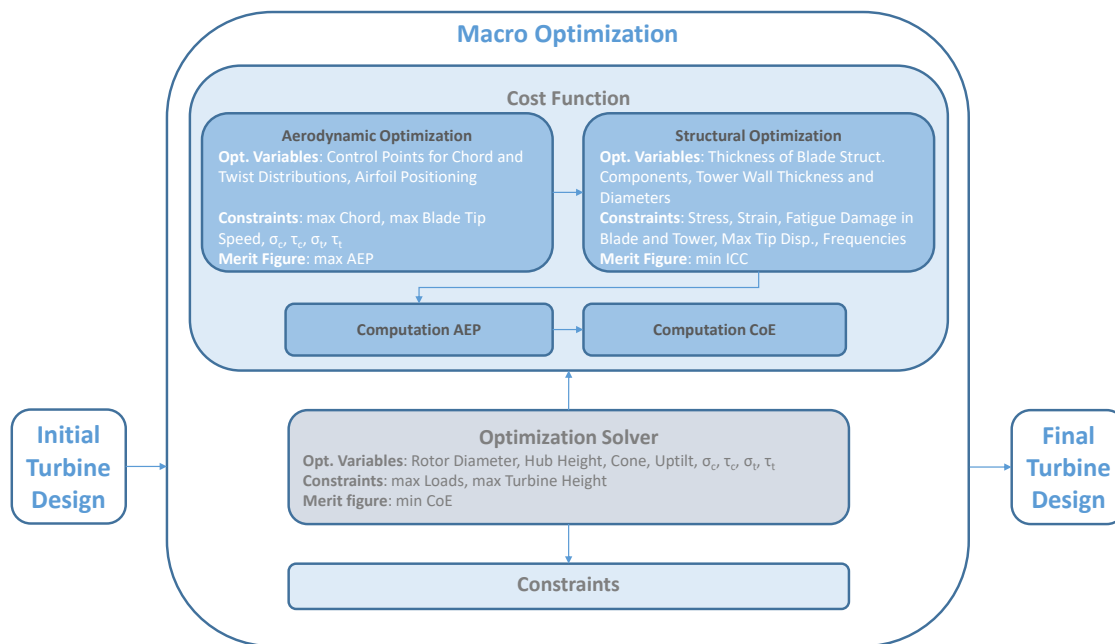


Figure 1. Scheme of the architecture of the design optimization procedure.

- Macro optimization - minimization of the Cost of Energy (CoE).

**Constraints:**

- Aerodynamic optimization - noise limitations, transportability and manufacturing limitations. These typically translate into maximum allowable values for blade tip speed, maximum value of the chord distribution, maximum variations along blade span of chord, twist and relative thickness. Aero-shape parameters from Eq. 1.
- Structural optimization - maximum allowable stress, strain and fatigue damage along blade and tower in a user-defined number of stations, maximum blade tip deflection, blade and tower frequency constraints to prevent modes coalescence and resonance effects, manufacturing limitations such as minimum and maximum thicknesses of composites and tower sectors as well as transportability constraints for the tower diameters.
- Macro optimization - extreme and fatigue load constraints in user-defined locations in the wind turbine, maximum turbine height.

The aerodynamic and structural loops are nested within the cost function of the macro optimization loop. For every call of the macro cost function, the code runs first the aerodynamic module, second the structural module, third the evaluation of the AEP under turbulent wind conditions and finally the computation of the CoE. This ensures that for every run of the macro cost function the aerodynamic and the structural optima are obtained and a consistent value of the CoE is computed. The aerodynamic and the structural loops are interconnected by the variables  $\sigma_c$ ,  $\tau_c$ ,  $\sigma_t$  and  $\tau_t$ , the four controlling the aerodynamic shape of the blade. The variables are defined as:

$$\sigma_c = \frac{3 \cdot A_b}{A} = \frac{3 \cdot \int_0^R c(r) dr}{\pi \cdot R^2}, \tag{1a}$$

$$\tau_c = \frac{\int_0^R r \cdot c(r) dr}{A_b}, \tag{1b}$$

$$\sigma_t = \frac{1}{100} \cdot \int_0^1 t(\eta) d\eta, \tag{1c}$$

$$\tau_t = \frac{\int_0^1 \eta \cdot t(\eta) d\eta}{\int_0^1 t(\eta) d\eta}, \tag{1d}$$

where  $A_b$  is the blade planar area,  $A$  is the rotor swept area,  $R$  the rotor radius,  $c$  the chord,  $r$  is the dimensional blade span,  $t$  is the blade percentage thickness and  $\eta$  the non-dimensional blade span. These four parameters act as optimization variables in the macro optimization loop and as non linear constraints in the aerodynamic optimization loop.

Finally, the outer macro optimization loop is subjected to the nonlinear constraints defined above. These directly influence the available solution space and are typically project specific. In this study, constraints on ultimate and fatigue loads at blade root, rotor shaft and tower top are considered.

All three optimization modules currently adopt a sequential quadratic programming (SQP) algorithm implemented in the MATLAB routine `fmincon` [10], where gradients are computed by means of central finite differences. However, this is partially an arbitrary choice and other optimization solvers could also be adopted, given however the compelling need of reducing the number of calls of the computationally expensive macro cost function.

In its formulation, `Cp-Max` calls a number of software. The core of the tool is the multibody based aeroservoelastic solver `Cp-Lambda` (Code for Performance, Loads, Aeroelasticity by Multi-Body Dynamic Analysis [11]). `Cp-Lambda` implements a complete library of elements, including non-linear flexible composite-ready beams, rigid bodies, joints, actuators and sensors. These elements can be arbitrarily combined and although `Cp-Max` can handle both upwind and downwind configurations equipped with an arbitrary number of blades modeled with an arbitrary number of beams and point masses, this study is limited to wind turbine modeled with the topological scheme shown in Fig. 2. `Cp-Lambda` is tightly coupled with aerodynamic models based on the classical blade-element momentum (BEM) approach, formulated according to the annular stream-tube theory with wake swirl, including tip and hub loss models, as well as unsteady corrections and dynamic stall.

Other software called within the tool are:

- ANBA (ANisotropic BeamAnalysis) - 2D finite element cross sectional analyzer implementing the theory of Giavotto et al. (1983) [12]. The solver computes the six-by-six stiffness matrix that defines the sectional characteristics at a given spanwise location of the geometrically exact shear and torsion-deformable beam model used in `Cp-Lambda`.
- Cost models - CoE models developed by NREL [13] and by the European INNWIND consortium [14] and detailed blade cost model developed by Johans and Griffith at SANDIA National Laboratories [15]. These cost models drive the optimization modules of `Cp-Max` and include all relevant items to compute the turbine capital cost (TCC) and the balance of stations (BoS), as well as produce an estimate for the operation and maintenance costs (O&M).
- MSC NASTRAN - commercial finite element solver for a detailed blade structural analysis [16]. The solver can be called by the user within the structural optimization module for a higher fidelity verification of the non-linear constraints. A full 3D-shell elements FE model is constructed, ran and post-processed in a completely automatic modality [17].
- TurbSim - stochastic, full-field, turbulent wind simulator [18]. The generated wind grids are used as input flow conditions during the computation of the dynamic aeroservoelastic simulations of `Cp-Lambda`.
- XFOIL - 2D panel code to compute subsonic performance of generic isolated airfoils [19];

Each software is called within the framework, which writes the necessary input files and automatically post-processes the outputs generating a fully automated simulation and design tool. It is also worth noting that the structure of the code is modular and each of this solver could be replaced with alternative software, if advantageous.

### 3. WIND TURBINE BASELINE DESIGN

The optimization work starts with the development of a class 3A onshore wind turbine model characterized by a rated mechanical power of 3.6 MW, a rated electrical power of 3.35 MW, a rotor diameter of 130 meter and a hub height of 110 meter. The activity falls within the framework of the IEA Wind Task 37 [9] and the goal of the design is to act as reference for future research projects on onshore wind energy. Indeed the size of the wind turbine has been selected by the project partners based on the consideration that this size is the one becoming the most common in the onshore wind energy market.

The starting point for the design process is an industrial 2 MW wind turbine described in Bortolotti et al., 2016a [3]. This model goes first through a manual resizing of hub, shaft, drive-train, nacelle and generator systems components. The values of volume and mass are scaled following the analytical relationships suggested by Guo et al., 2015 [20] and are reported in Table I. In addition, the airfoils listed in Table II are assumed as input for the aerodynamic optimization solver, which can then automatically position the profiles along blade span to maximize the AEP. Finally, blade root diameter is increased from 1.9 to 2.6 meters. On the structural side, the composites adopted in the inner structure of the blade are updated to materials adopted in the blades of the INNWIND 10 MW [21]. In terms of blade topology, the structural components are the same as in the 2 MW design, but the chordwise positioning of spar caps and webs is scaled linearly with the rotor diameter. This data is summarized in Table III. Moreover, a lower bound for the composite laminate at blade root of 80 mm is assumed to allocate the blade root bolts. Lastly, a set of critical design load cases (DLCs) is generated for load assessment, including standard operating conditions under normal turbulence model (1.1), operation under extreme turbulence model (1.3), shut down cases under turbulent wind (2.1) and steady wind with gusts (2.3), and finally storm conditions (6.1, 6.2, 6.3) [6]. Each class of DLCs includes three turbulent seeds for a total of 151 dynamic simulations.

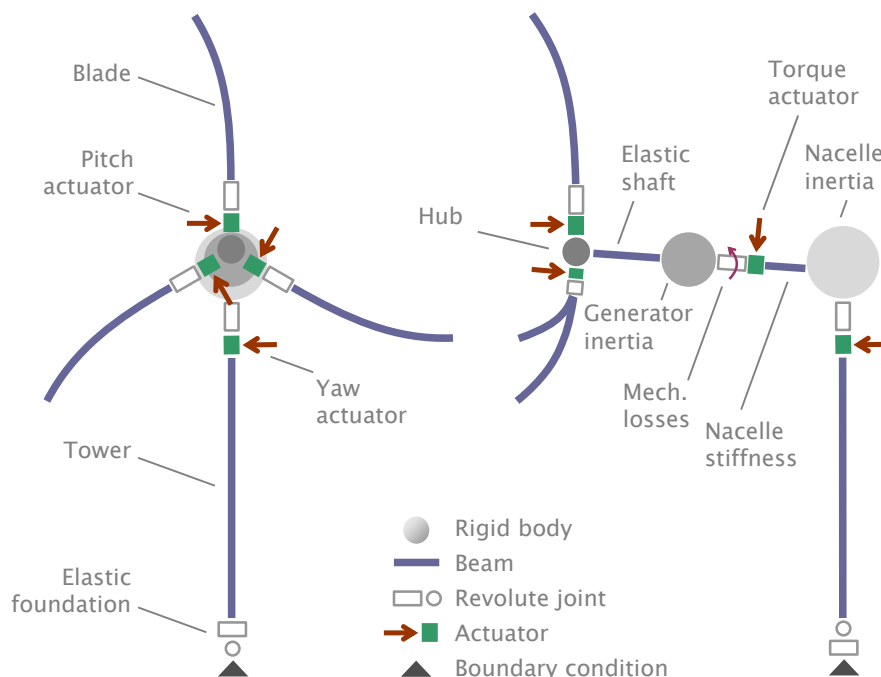


Figure 2. Topological scheme of the wind turbine model constructed in  $C_p$ - $\Lambda$ mbda.

Table I. Scaling of hub, shaft, drive-train, generator and nacelle.

Component	Mass		Inertia	
	2 MW	3.35 MW	2 MW	3.35 MW
Hub	27000 kg	55000 kg	About shaft axis	19100 kg · m <sup>2</sup>
			Off shaft axis	86000 kg · m <sup>2</sup>
Nacelle	21750 kg	46500 kg	About yaw axis	355000 kg · m <sup>2</sup>
			Generator	50000 kg
Generator	50000 kg	80600 kg	Off shaft axis	24720 kg · m <sup>2</sup>
				61584 kg · m <sup>2</sup>

Table II. Airfoils adopted during the design development.

Airfoil	Thickness	Airfoil	Thickness
Circle	0.0%	DU00-W2-401	40.1%
DU00-W2-350	35.5%	DU97-W-300	30.0%
DU91-W2-250	25.1%	DU08-W-210	21.0%
DU08-W-180	18.0%		

The aerodynamic design comprises 24 optimization variables describing twist at eight stations, chord at nine stations and the position of the seven airfoils along blade span. The structural design is made of 50 variables parameterizing the skin, the two spar caps, the two webs and the leading and trailing edge reinforcements in nine stations along blade span, as well as diameter and wall thickness of ten tower sectors. In this exercise, the mechanical properties of the composites are kept fixed, while sweep curvature, angles in the composite fibers and offset in the spar cap positioning are all set to zero.

Based on all these assumptions and a maximum tip speed of 80 m/s,  $C_p$ -Max is run to find the aero-structural design producing the lowest CoE. After a total computational time of approximately 100 hours running on a workstation equipped with 56 logical processors,  $C_p$ -Max converges to the solution that is summarized in Table IV. The chord, twist, relative thickness and prebend distributions along blade span are reported in Fig. 3, while the details of the structural design of blade and tower are reported in Fig. 4. In terms of blade outer shape, it is worth noting that chord and prebend, reported in Fig. 3a and 3d respectively, are highly constrained by maximum allowable values of 5 meters and 2.5 meters respectively,

**Table III.** Extent of the blade structural components and corresponding composites.

Component	From (% span)	To (% span)	Material type	Longitudinal Young's modulus [MPa]	Transversal Young's modulus [MPa]	Shear modulus [MPa]
Outer shell	0	100	Stitched triaxial -45°/0°/+45° fiberglass	21790	14670	9413
Spar caps	10	96	Unidirectional fiberglass	41630	14930	5047
Shear webs	10	96	Stitched biaxial -45°/+45° fiberglass	13920	13920	11500
Trailing and leading edge reinforcements	10	80	Unidirectional fiberglass	41630	14930	5047
Sandwich core	5	96	Balsa	50	50	150

**Table IV.** Configuration of the baseline wind turbine.

Data	Value	Data	Value
Wind class	IEC 3A	Rated aerod. power	3.6 MW
Rated electr. power	3.35 MW	DT & Gen. efficiency	93.0%
Hub height	110.0 m	Rotor diameter	130.0 m
Cut-in	4 m/s	Cut-out	25 m/s
Rotor cone	3.0 deg	Nacelle uptilt	5.0 deg
Rotor solidity	4.09 %	Max $V_{tip}$	80.0 m/s
Blade mass	17525 kg	Tower mass	365 ton
Blade cost	127.9 k\$	Tower cost	548.5 k\$
A. AEP	15.01 GWh	Electr. AEP	13.96 GWh
ICC	3885.2 k\$	CoE	42.00 \$/MWh

which are assumed to ensure transportability. In addition, it is worth highlighting that the optimizer discards the profile DU08-W-180, favoring the thicker airfoils. As visible in Fig. 3c, the minimum relative thickness along the blade is indeed 21%, value that guarantees a better trade-off between aerodynamic and structural performance. On the blade structural side, the constraints driving the design are maximum allowable tip deflection and frequency. In addition, the fatigue constraint is active at convergence in the shell skin in the mid-span of the blade. In the tower, fatigue is highly dominant in all ten sectors, where the outer diameter reaches its upper bound set at 8 meters in the three sectors closest to ground. The final design, which is available for all partners of the IEA Wind Task 37, produces an expected value of CoE calculated from the NREL cost model equal to 42.00 \$/MWh.

#### 4. LOAD ALLEVIATING ROTOR DESIGN

Wind turbines have seen a steady increase in size in the last decades. This growth is motivated by the need to decrease the CoE, where the easiest way to achieve this is to increase the energy capture while limiting the cost of the machine. Indeed, since the efficiency of modern multi-MW machines can only be marginally improved, the best approach to increase AEP is to adopt larger rotor swept areas. However, while doing so the simple upscaling of existing rotors is hindered by the cubic law of growth: scaling up a rotor by a given factor increases its volume, hence typically its weight and cost, by the cube of that factor.

The adoption of load alleviating techniques typically helps in reducing the exponent guiding the cost increase and the importance of load alleviation technologies is widely recognized as witnessed by the large body of literature and research projects dedicated to this topic [21, 22, 23]. The current work specifically targets the evaluation of upwind wind turbine design adopting passive load alleviation technologies with no moving parts. These solutions are very attractive because of their very nature: there are no actuators that may fail and no need for sensors. In the recent literature, several of them

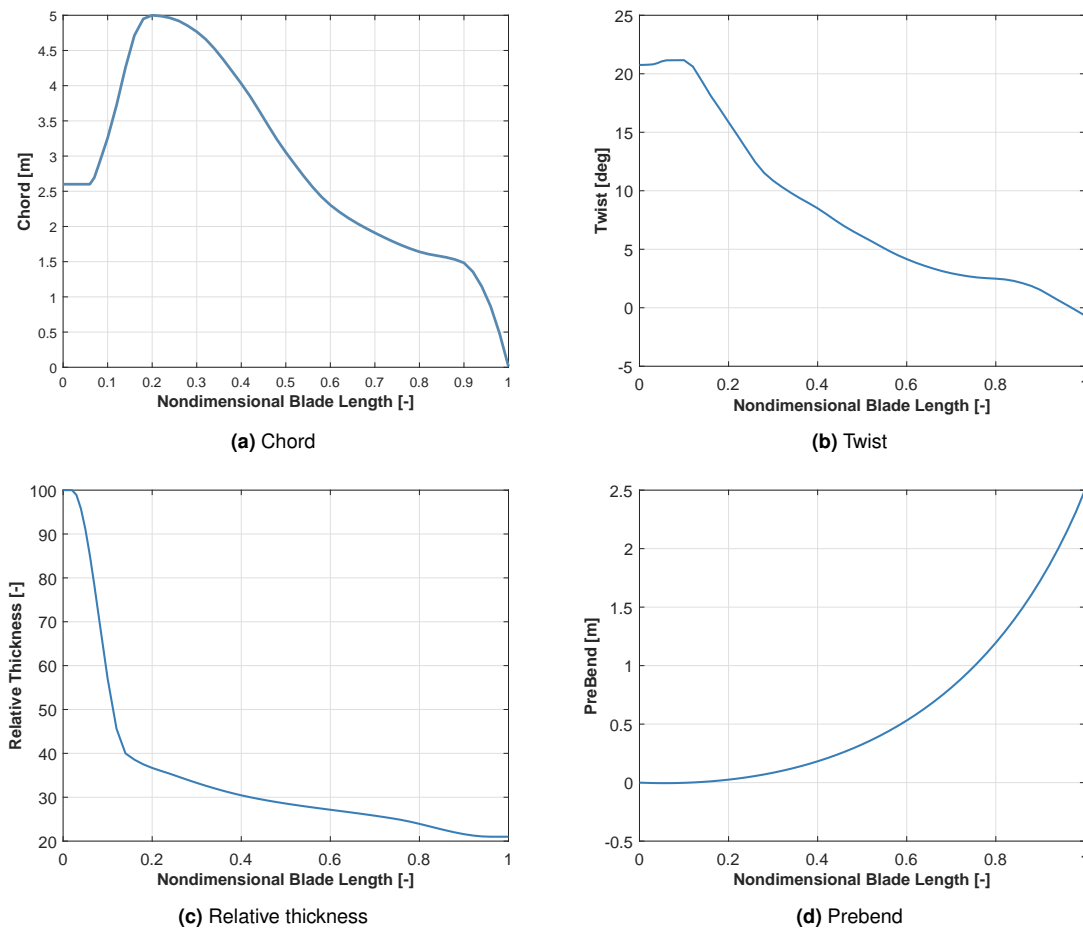


Figure 3. Aerodynamic blade shape of the baseline wind turbine.

have been described. The classical solution to achieve this load reduction behavior has been to design blades with some degree of bend-twist coupling (BTC). In fact, BTC implies that when the blade bends because of increased loads, the ensuing change of twist affects the aerodynamic loading through a change in angle of attack  $\alpha$ . This change in  $\alpha$  can be either positive or negative generating twist to stall or twist to feather mechanisms. The latter is typically preferred in large modern blades and it is here investigated.

Passive load mitigation by BTC can be obtained by exploiting the anisotropic mechanical properties of composite materials [24, 25], or by sweeping the blade [26, 27]. The first technological solution will be here referred as F-BTC (for fiber-induced BTC), while the second will be called S-BTC (for sweep-induced BTC). More recently, it was found that also dislocating the spar caps between suction and pressure sides of the blade may achieve a similar result [28]. This offsetting of the spars also typically requires an equivalent offset in the positioning of the shear webs and will be here referred as offset BTC, therefore listed as O-BTC.

Although these passive load alleviation technologies have been individually investigated in details, it is only recently that research projects are also looking into a combination of each technique [25, 29]. This work aims at running a consistent comparison aiming at an integration of the different techniques. The baseline wind turbine is then here adopted as starting point for three studies to individually investigate the passive load alleviation solutions to later look for potential benefits generated by a merging of the three technologies. A parametric study on S-BTC is first performed and exposed in Sect. 4.1. Secondly, Sect. 4.2 reports results generated from a parametric study on F-BTC. Third, O-BTC is analyzed under different values of offsets in the position of suction and pressure spar caps as well as shear webs. This study is shown in Sect. 4.3. After the parametric studies, a regulation trajectory for BTC rotors is presented in Sect. 4.4. Finally, the optimization algorithms of  $C_p$ -Max are run aiming at an automatic identification of an overall optimum wind turbine configuration under the constraints of maximum allowable ultimate and fatigue loads measured in several locations such as blade root, hub and nacelle system. This last study is presented in Sect. 4.5.

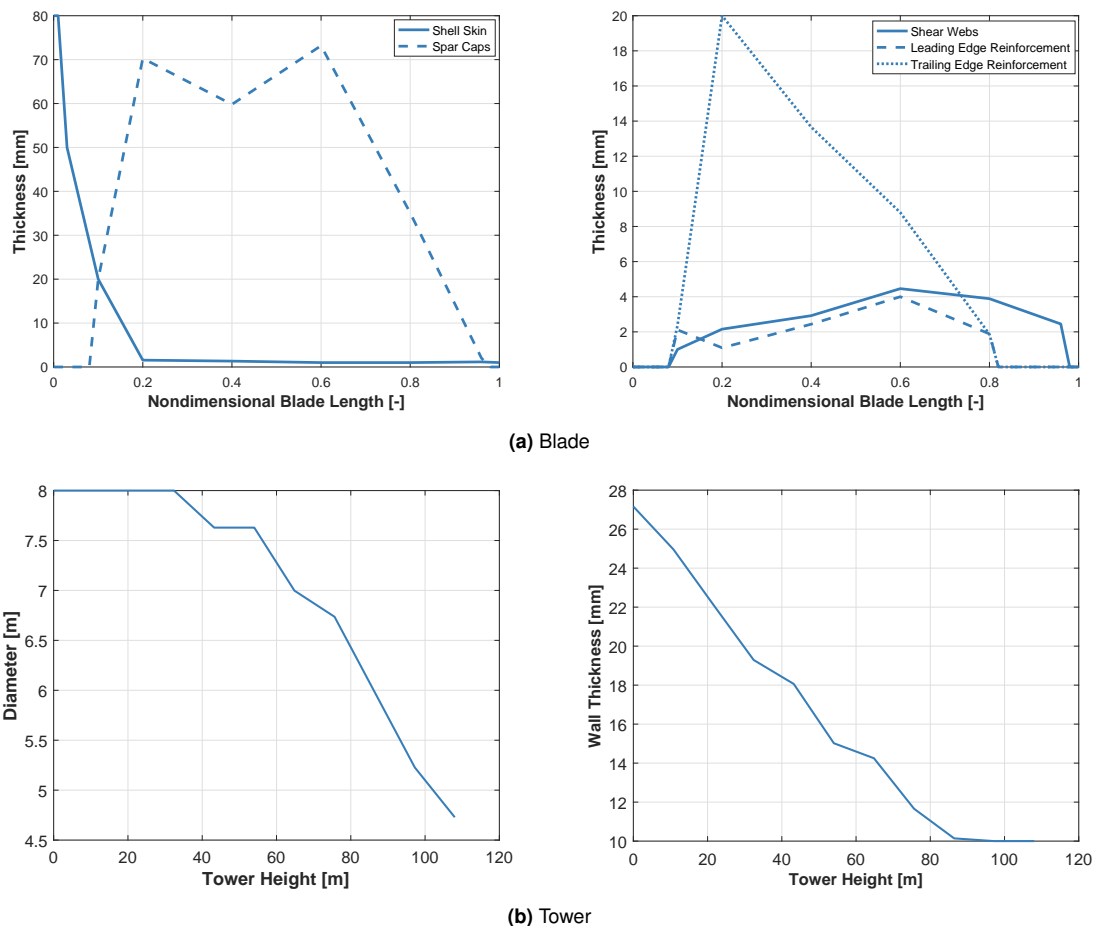


Figure 4. Structural design of blade and tower of the baseline wind turbine.

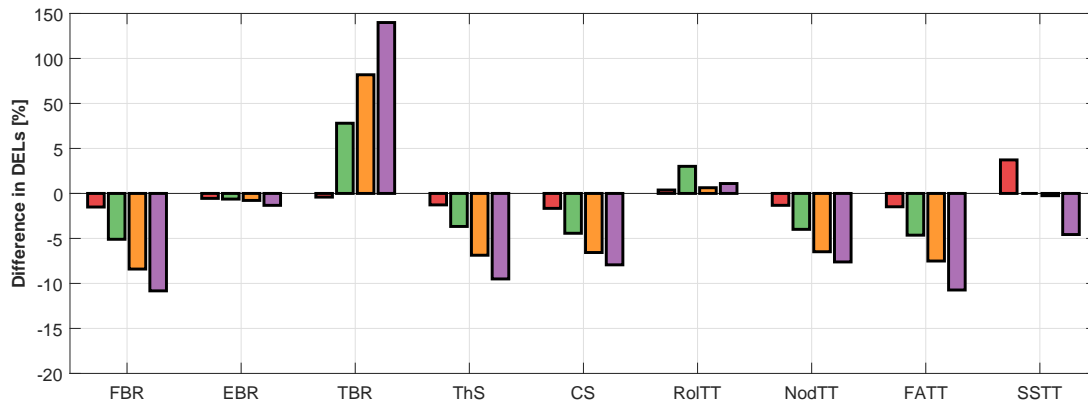
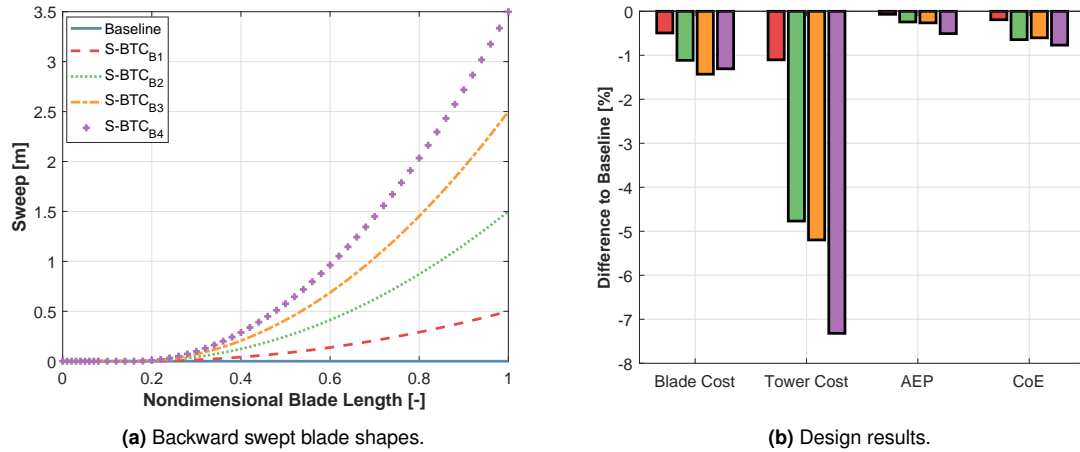
### 4.1. Swept rotor blades S-BTC

Sweep is the curvature of the blade axis in the rotor plane. Swept blades have the potential advantage of an induced BTC kinematic effect due to the generated torsional forces. Arbitrary curvatures can be defined in  $C_{p-Max}$ , but in this study the family of curvatures defined by Eq. 2 [27] are first assumed:

$$y = d_{tip} \cdot \left( \frac{x - x_{start}}{(R_{rotor} - R_{hub}) - x_{start}} \right)^\gamma \tag{2}$$

where  $y$  is the local distance from pitch axis to sweep curve,  $x$  is the radial coordinate along the pitch axis,  $R_{rotor}$  and  $R_{hub}$  are the radii of wind turbine rotor and hub respectively,  $d_{tip}$  is the distance of blade tip to pitch axis,  $x_{start}$  is the start position of sweep and finally  $\gamma$  is the exponent governing the sweep curvature.

Preliminary tests show the highest sensitivity of CoE to  $d_{tip}$  and this variable is chosen to be varied parametrically, while  $x_{start}$  and  $\gamma$  are assumed to be 10 meters and 2 respectively. A value of 3.5 meters is assumed as maximum for  $d_{tip}$  to respect realistic limitations on blade transportability. Under these assumptions, the set of backward swept blade shapes, named S-BTC<sub>B1</sub>, S-BTC<sub>B2</sub>, S-BTC<sub>B3</sub> and S-BTC<sub>B4</sub> (where B stands for Backward sweep), is generated assuming values of  $d_{tip}$  of 0.5, 1.5, 2.5 and 3.5 meters respectively. The backward sweep curvatures are shown in Fig. 5a. Each blade goes then through an aerodynamic optimization to find the optimum twist distribution at rated conditions and a structural optimization for blade and tower. Sweep is confirmed to be effective in significantly reducing both blade tip displacements during turbulent gusts as well as the overall fatigue damage on both blades and tower. This results in mass and cost savings in the blade and in the tower as shown in Fig. 5b. Moreover, thanks to the adjusted twist following the new torsional deformations of each blade design, the losses in energy production, which is estimated during DLC 1.1 under turbulent wind conditions, can be limited within 0.5%. This results in CoE savings up to 0.8%. In addition, as shown in Fig. 5c



(c) Difference in DELs along wind turbine. DELs are computed at Wöhler fatigue exponent and number of cycles equal to 4 and  $10^7$  respectively. Legend: FBR - Flapwise Blade Root Moment, EBR - Edgewise Blade Root Moment, TBR - Torsional Blade Root Moment, ThS - Thrust at Shaft, CS - Combined Moment at Shaft, RoITT - Rolling Moment at Tower Top, NodTT - Nodding Moment at Tower Top, FATT - Fore-Aft Force at Tower Top, SSTT - Side-Side Force at Tower Top.

Figure 5. Results of backward sweep parametric study.

sweep generates a strong reduction in fatigue damage equivalent loads (DEL) in several locations of the machine except for the blade root torsional moment.

A parametric study is then conducted by introducing a forward component in Eq. 2:

$$y = (d_{tip} + y_{min}) \cdot \left( \frac{x - x_{min}}{(R_{rotor} - R_{hub}) - x_{min}} \right)^\gamma - y_{min} \quad (3)$$

where  $y_{min}$  is the absolute value of forward sweep at the span position  $x_{min}$ . A small sub-optimization module is implemented to identify the values of  $y_{min}$  that for given  $\gamma$  and  $d_{tip}$  generate null blade root torsional loads under static loads at rated conditions. For every value of  $y_{min}$ ,  $x_{min}$  is adjusted to guarantee a value of 0 meters of sweep at blade root. This sweep balancing module is tested for values of  $\gamma$  and  $d_{tip}$  equal to 2 and 3.5 meters respectively, generating the blade here called S-BTC<sub>BC</sub> (where BC stands for Balanced Centered sweep), which is characterized by values of  $y_{min}$  and  $x_{min}$  of 0.44 and 16.4 meters respectively. In addition, as a comparison two more blades shapes are generated using Eq. 3 adopting values of  $y_{min}$  of 0.40 and 0.70 meter and values of  $x_{min}$  of 16.0 and 19.0 meters. These two blades are referred as S-BTC<sub>C1</sub> and S-BTC<sub>C2</sub> (where C stands for Centered sweep). The three blades are redesigned in terms of twist and structure, generating the results reported in Fig. 6. As visible in Fig. 6b, S-BTC<sub>BC</sub> proves successful in limiting the growth in fatigue torsional loads at blade root to 75% against 140% of S-BTC<sub>B4</sub>.

Overall, blade solutions characterized by a swept plan form generate a positive reduction in blade deflections and fatigue loads thanks to the BTC effect. This results in savings in the mass and cost of rotor and tower and it generates room for a growth in rotor size at constant baseline loads. In addition, the method to balance statically forward and backward sweep

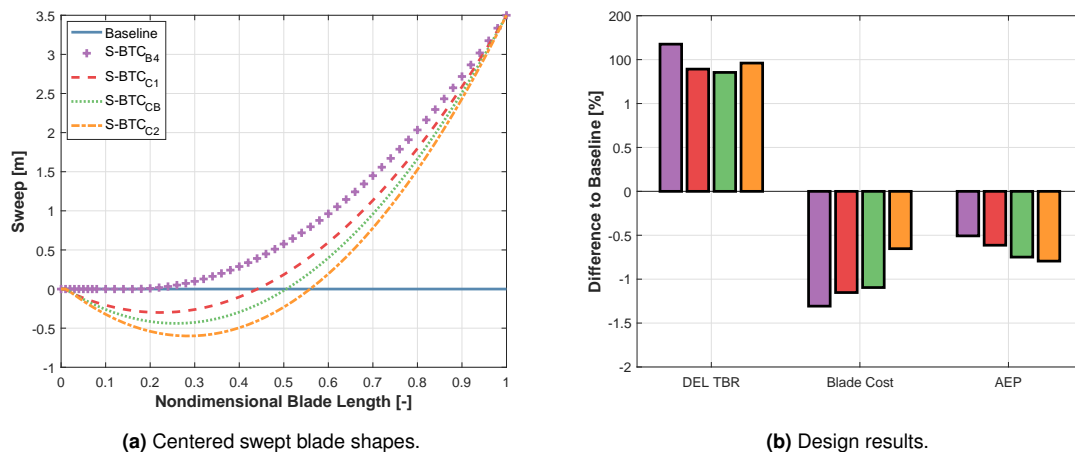


Figure 6. Results of centered sweep parametric study.

distribution helps in limiting the growth in torsional loads on the pitch system. These aspects are further investigated in Sect. 4.5.

#### 4.2. Composite fibers misalignment F-BTC

This study follows the path drawn by Bottasso et al., 2013 [25] assessing the impact of inclined fabrics on the rotor blade design, extending the analysis to the effects on the tower structure. Two parametric analyses varying the angle in the fibers of the spar cap laminates are first conducted. First, four design studies are run with an angle in the fibers of 2.5, 5.0, 7.5 and 10.0 degrees. These are here listed as F-BTC<sub>SC1</sub>, F-BTC<sub>SC2</sub>, F-BTC<sub>SC3</sub> and F-BTC<sub>SC4</sub> (where <sub>SC</sub> stands for Spar Cap misaligned fibers). A visual summary of the results is reported in Fig. 7. Simulations return a slight growth in blade mass and cost due to the loss of bending stiffness caused by the misaligned laminates and a more marked drop in tower mass and cost thanks to the consistent reduction in fatigue load. In addition, a loss in AEP is measured as in Sect. 4.1 and the overall effect is an overall null or very limited effect on the CoE.

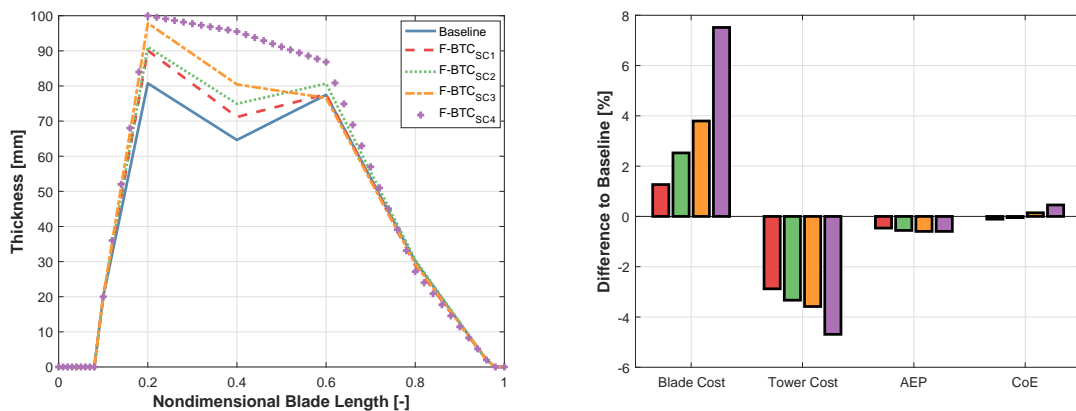
In a second parametric analysis, three more blades are designed simulating a spar cap split in two portions, adopting a constant fiber misalignment of 0 degrees in the section towards the root and a misalignment of 10 degrees in the outer blade span. Three values for the position of the change in fiber angle along blade span are assumed at 50%, 62.5% and 75%, generating the blades here called F-BTC<sub>PSC1</sub>, F-BTC<sub>PSC2</sub> and F-BTC<sub>PSC3</sub> (where <sub>PSC</sub> stands for Partial Spar Cap). Simulations return intermediate values between the baseline wind turbine configuration and the solution with the entire spar cap adopting twisted fibers.

A third study is performed on the re-orientation of the outer shell skin laminate. To successfully induce an F-BTC effect, it is here necessary to replace the baseline triaxial laminate due to its very mild anisotropy. The triaxial of the original 2.0 MW blade is then modeled generating the blade here called F-BTC<sub>SK1</sub> (where <sub>SK</sub> stands for Shell Skin). The laminate is then misaligned by 10 and 20 degrees creating the blades F-BTC<sub>SK2</sub> and F-BTC<sub>SK3</sub> respectively. By simply adopting the new laminate, the rotor returns a benefit in blade mass and cost of 6.3% and 1.4% respectively, while misaligned fibers generate a BTC effect.

Table V returns all the blade design solutions generated during the study on F-BTC. Overall, numbers show that as long as the rotor size is not increased, rotors equipped with F-BTC do not look markedly advantageous in terms of CoE compared to traditional configurations. Nevertheless, F-BTC generates marked reductions in fatigue load reductions and, similarly to S-BTC, this allows the possibility to increase rotor size and therefore power capture without increasing fatigue loads. In addition, several F-BTC configurations return similar load alleviation effects and it is therefore conceivable to simultaneously combine a misalignment in both spar cap and outer shell skin. This in turn offers the possibility to adopt smaller angles in each component, which may result in benefits from manufacturing as well as off-axis stress conditions within the laminates. A setup with an angle of 5 and 10 degrees in spar caps and shell skin respectively is then investigated in Sect. 4.5.

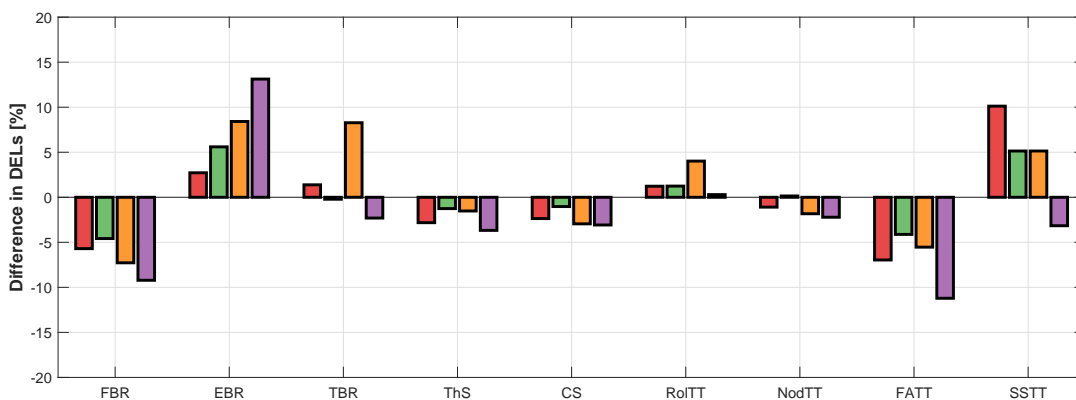
#### 4.3. Offsetting the position of spar caps and shear webs O-BTC

Inspired by the promising results obtained on the INNWIND 10 MW rotor [28, 29], a last parametric study is conducted on O-BTC investigating the effects of the positioning of the shear webs as well as of the spar caps on the suction and on



(a) Spar caps thickness at varying fibers angle.

(b) Design results.



(c) Difference in DELs along wind turbine. Legend see Fig .5.

Figure 7. Results of spar cap fiber angle parametric study.

Table V. Comparison between F-BTC design solutions.

Component	Angle	Difference to baseline				
		DEL FBR	Blade cost	Tower cost	AEP	CoE
<b>Spar caps</b>						
F-BTC <sub>SC1</sub>	2.5 deg	-5.7 %	+1.3 %	-2.9 %	-0.46 %	-0.11 %
F-BTC <sub>SC2</sub>	5.0 deg	-4.6 %	+2.5 %	-3.3 %	-0.56 %	-0.05 %
F-BTC <sub>SC3</sub>	7.5 deg	-7.3 %	+3.8 %	-3.6 %	-0.60 %	+0.14 %
F-BTC <sub>SC4</sub>	10.0 deg	-9.2 %	+7.5 %	-4.7 %	-0.60 %	+0.46 %
<b>Partial spar caps</b>						
F-BTC <sub>PSC1</sub>	10.0 deg from 50.0 % span	-5.9 %	+3.6 %	-5.0 %	-0.48 %	-0.09 %
F-BTC <sub>PSC2</sub>	10.0 deg from 62.5 % span	-4.0 %	+1.8%	-3.0 %	-0.32 %	-0.10 %
F-BTC <sub>PSC3</sub>	10.0 deg from 75.0 % span	-1.6 %	+0.6%	-1.5 %	-0.16 %	-0.08 %
<b>Outer shell skin</b>						
F-BTC <sub>Sk1</sub>	0.0 deg	-3.8 %	-1.4 %	0.0 %	-0.04 %	-0.21 %
F-BTC <sub>Sk2</sub>	10.0 deg	-2.0 %	-2.2 %	-1.5 %	-0.20 %	-0.37 %
F-BTC <sub>Sk3</sub>	20.0 deg	-4.0 %	-2.3 %	-1.3 %	-0.29 %	-0.34 %

the pressure sides of the blade. Such change in blade internal geometry induces a coupling between flapwise and edgewise

bending generating a swept shape when blades are loaded. Several combinations of offsets in the spar caps only and in spar caps and shear webs together are investigated at different offset values imposed both at the tip or along the whole span of the blade.

Differently from the results obtained from the 10 MW rotor, here results do not prove particularly promising and the main reason is identified in the fact that offset values only up to 250 mm can be modeled in large blade portions due to the pronounced blade slenderness combined with relatively large spar caps. This strongly limits the flap-edge coupling effects that can be generated. These are then negatively compensated by the loss in blade flapwise stiffness caused by the asymmetric placement of the spar caps and the resulting O-BTC blade design solutions produce either null or very limited ultimate and fatigue load reductions, while increasing blade cost and decreasing AEP. As a conclusion, O-BTC designs are here not adopted further.

#### 4.4. Regulation trajectory for BTC rotors

A traditional controller of wind turbines operates the machine across regions I, II, II $\frac{1}{2}$ , III and IV, where each region is characterized by a different logic:

- Region I: the machine idles due to wind speeds below cut in wind speed  $V_{cut\ in}$ .
- Region II: the machine operates at fixed pitch angle  $\beta$  and tip speed ratio  $\lambda$  aiming at maximum aerodynamic performance.
- Region II $\frac{1}{2}$ : to limit aerodynamic noise emissions, a constraint on the maximum allowable value of blade tip speed is imposed. The wind turbine operates at constant rotor speed causing a suboptimal  $\lambda$ . The power coefficient  $C_p$  is maximized for the given  $\lambda$ .
- Region III: the machine operates at constant rotational speed, constant torque and variable  $\beta$  preventing the output power to exceed the rated value.
- Region IV: the machine is shut down due to wind speeds above the cut out wind speed  $V_{cut\ out}$ .

As visible in Figs. 5b and 7b as well as in Table V, BTC rotors typically suffer a loss in energy production compared to the baseline rotor. This loss is mostly generated in region II, where a regulation strategy with constant  $\beta$  guarantees optimal performance for torsionally stiff blades, but shows its limits in presence of BTC rotors that see different torsional deformations and consequently different angles of attack under different loading. The solution to this problem is found by implementing a new regulation trajectory that schedules variable  $\beta$  and  $\lambda$  both above and below rated conditions.

The new regulation trajectory is tested comparing its performance on the baseline configuration and on the S-BTC<sub>B3</sub> rotor. Figure 8 reports the different behaviors for  $\beta$  in Fig. 8a,  $\lambda$  in Fig. 8b and the resulting  $C_p$  in Fig. 8c. As expected, minor differences are observed in the baseline rotor between the traditional and the new regulations strategies. Indeed the baseline rotor has only a minimal BTC, which is simply caused by the non symmetric and flexible structure, and this means that the blades do not significantly twist while bending. On the opposite, much more marked advantages are found in the S-BTC<sub>B3</sub> rotor, whose aerodynamic performance suffers the sub-optimal angles of attack in region II. Thanks to the varying  $\beta$ , it is now possible to partially recover the loss in energy production generated by the BTC effect. Indeed, as reported in Fig. 8d, thanks to the varying  $\beta$ , the S-BTC<sub>B3</sub> rotor cuts the loss in AEP from -0.42% to -0.28% when nominal conditions are assumed and from -0.79% to -0.42% when AEP is estimated from the dynamic conditions of three turbulent wind seeds of DLC 1.1.

A drawback of such change in regulation trajectory is an increase in the actuator duty cycle (ADC) of the pitch actuator. The ADC is here defined as the Weibull weighted ratio of pitch rate over maximum pitch rate integrated over time:

$$ADC = \int_{V_{cut\ in}}^{V_{cut\ out}} \left( f_w(V) \cdot \frac{1}{T} \cdot \int_0^T \left( \frac{\dot{\beta}(t, V)}{\dot{\beta}_{max}} \right) dt \right) dV \quad (4)$$

where  $f_w$  is the Weibull probability density of each wind speed,  $T$  is the duration in seconds of each dynamic simulation,  $\dot{\beta}$  is the pitch rate and  $\dot{\beta}_{max}$  is the maximum allowable pitch rate. Here ADC is estimated during DLC 1.1 with three turbulent wind seeds.

This growth does appear in the results, where the ADC of the new regulation trajectory for the S-BTC<sub>B3</sub> is higher than the ADC required by the original regulation trajectory. Nevertheless, thanks to the bend-twist effect, BTC rotors do require a slightly smaller ADC compared to conventional non-BTC rotors [25] and overall the ADC of the S-BTC<sub>B3</sub> rotor is only 0.9% higher than the ADC of the reference configuration. In conclusions, it is found that the new regulation trajectory is beneficial for BTC rotors, and it is therefore adopted for the subsequent study.

#### 4.5. F-S-BTC enlarged rotor

As a last step of the study, a rotor redesign exercise is defined investigating the optimum rotor and tower configuration that minimizes CoE and that generates the same list of ultimate and fatigue loads reported in Table VI and experienced by the baseline wind turbine model. In the exercise, the constraint on the first natural frequency of the blade, which typically

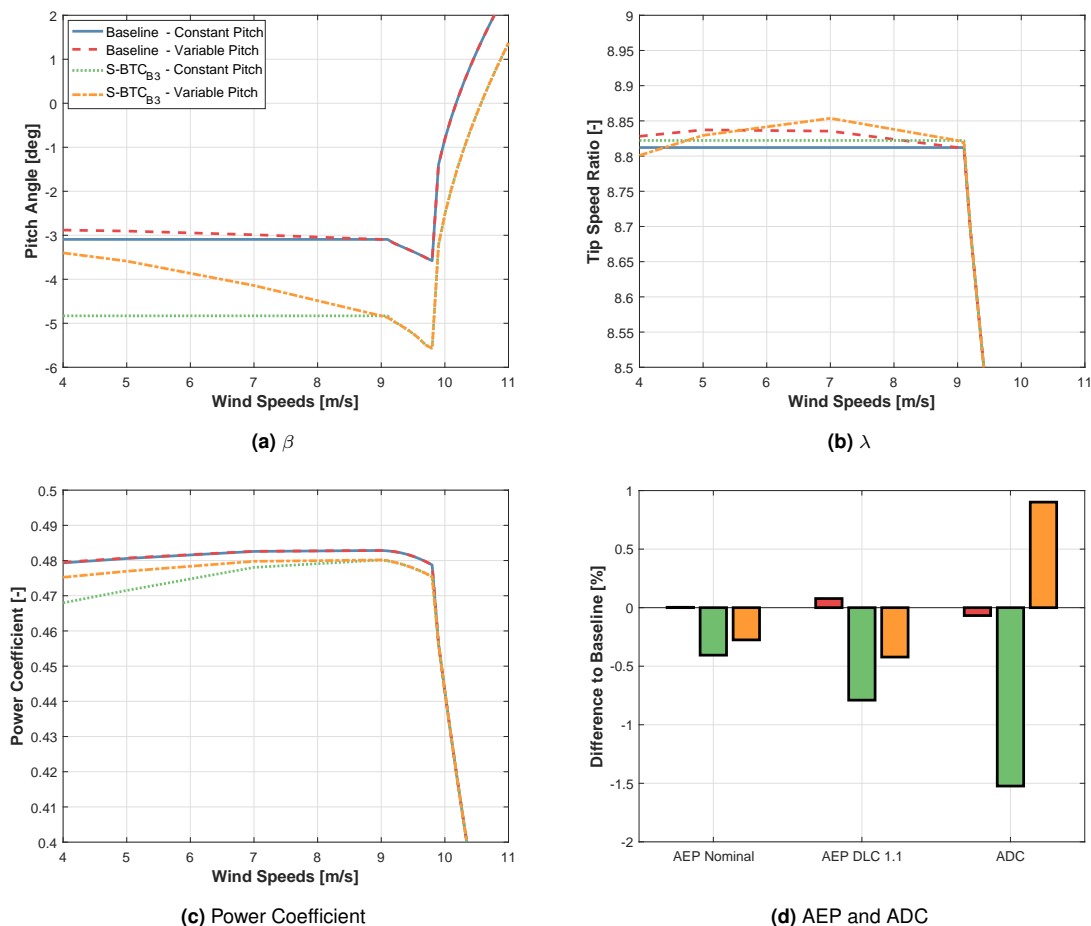


Figure 8. Comparisons of regulation trajectories for the baseline rotor and S-BTC<sub>B3</sub>.

prescribes that the first natural frequency of the blade has to be at least 16% higher than the 3P harmonics of the system, is also removed. In addition, a blade tip sweep of 3.5 meters is assumed and the procedure for sweep balancing described in Sect. 4.1 is used, while the initial triaxial composite adopted in the outer shell skin is changed to the one tested in Sect. 4.2 and angles of 5 and 10 degrees are adopted in the orientation of the laminates in the spar caps and in the outer shell skin respectively. Finally, varying pitch is adopted in all regions II, II<sub>1/2</sub> and III as in Sect. 4.4.

After a computational time of 80 hours, results return the possibility to increase the rotor diameter to 136 meters while respecting all optimization constraints within a tolerance of 1%. This is obtained thanks to a wind turbine design solution radically different from the previous configuration. Indeed, the code indicates the combination of higher nacelle up tilt and rotor cone angles, increased to 6 and 8 degrees respectively, and very soft, flexible and light blades as optimum. Thanks to a drop in blade mass of 16.9%, the DELs measured at pitch and main bearings do not suffer any growth and the final wind turbine design, whose macro parameters are reported in Table VII, captures 2.6% more AEP, lowers the ICC by 0.9% and ultimately reduces the CoE by 2.8%.

Notably,  $C_p$ -Max does not change the aerodynamic shape of the blade during the optimization and a sensitivity analysis is then conducted to manually explore the solution space in terms of  $\sigma_c$ ,  $\tau_c$ ,  $\sigma_t$  and  $\tau_t$ . The study returns a very large plateau, with several solutions that reach an equilibrium in terms of CoE thanks to counterbalancing ICC and AEP. In addition, a sensitivity study is conducted on the cone angle to evaluate its effect on the CoE and very similar CoE values for wind turbines characterized by cone angles between 6 and 10 degrees are found. Below this range, simulations return the insurgence of resonance effects on the rotor due to the vicinity of the 3P harmonic of the system and the rotor out-of-plane collective frequencies. Indeed, cone angles smaller than 6 degrees rapidly cause a reinforcement of the tip deflection constraint and consequently lead to blades stiffer in flapwise direction. The room for an upward shifting of the natural frequencies of the rotor while avoiding the harmonics is however limited. Therefore, to prevent the negative effects caused by resonance, the gradient-based optimizer automatically jumps back to a traditional rotor configuration. On the opposite,

**Table VI.** Maximum allowable loads adopted as constraints. Legend see Fig .5.

Constraints on ultimate loads					
Load component	FBR	EBR	TBR	ThS	CS
Value	13.51 MNm	6.84 MNm	0.29 MNm	0.834 MN	8.81 MNm
Enforced	yes	yes	no	yes	yes
Load component	RoTT	NodTT	FATT	SSTT	
Value	4.69 MNm	7.42 MNm	0.75 MN	0.48 MN	
Enforced	yes	yes	yes	yes	
Constraint on fatigue DEL @ $N=10^7$ , Wöhler exponent $m=4$					
Load component	FBR	EBR	TBR	ThS	CS
Value	6.61 MNm	13.34 MNm	0.08 MNm	0.26 MN	6.02 MNm
Enforced	yes	yes	no	yes	yes
Load component	RoTT	NodTT	FATT	SSTT	
Value	1.45 MNm	6.10 MNm	0.36 MN	0.27 MN	
Enforced	no	yes	yes	yes	

**Table VII.** Comparison between the baseline design and the optimum configuration presented in Sect 4.5.

Data	Baseline	F-S-BTC Optimum	Difference
Rotor diameter	130.0 m	136.0 m	+4.6 %
Rotor cone	3.0 deg	8.0 deg	+166.7 %
Rotor uptilt	5.0 deg	6.0 deg	+20.0 %
Blade mass	17525 kg	14560 kg	-16.9 %
Blade cost	127.9 k\$	126.2 k\$	-1.3 %
Tower mass	365 ton	292 ton	+20.0 %
Tower cost	548.5 k\$	438.2 k\$	+20.1 %
Mech. AEP	15.01 GWh	15.40 GWh	+2.6 %
Electr. AEP	13.96 GWh	14.32 GWh	+2.6 %
ICC	3885.2 k\$	3850.9 k\$	-0.9 %
CoE	42.00 \$/MWh	40.82 \$/MWh	-2.8 %

between 6 and 10 degrees the CoE is predicted to be very close to the design solution automatically identified by  $C_p\text{-Max}$ . Within this range AEP suffers a gradual decrease, but blades and tower benefit from lower loads generating lower costs. Ultimate and fatigue loads are also lowered in several components of the wind turbine. Nevertheless, above a cone angle of 10 degrees the loss in AEP cannot longer be compensated by the savings in ICC, and CoE does show a steep increase.

It should be here remarked that the optimizer identifies this solution based on the list of constraints of Table VI, which is a fairly arbitrary choice. Other constraints would lead to other solutions, potentially very different from the one here identified. One of the biggest advantages of adopting automated systems engineering tools is indeed the capacity to generate a large number of design solutions in a matter of hours with little burden for the wind turbine designer.

## 5. CONCLUSIONS AND FUTURE WORK

This paper has presented the latest advancements in the wind turbine design methodologies implemented in the tool  $C_p\text{-Max}$  and their application to design modern multi-MW onshore wind turbines equipped with and without passive load alleviation techniques. Several studies are run and compared and the main conclusions are here summarized:

- Baseline configuration - a 3.35 MW onshore wind turbine design is developed thanks to an integrated wind turbine design optimization process and made public within the framework of the IEA Wind Task 37. The design, which is not equipped with load alleviating solutions, is consistently adopted as reference for all subsequent studies.

- Swept rotor blades S-BTC - different swept rotor configurations are designed and compared, returning lower loads and CoE. Thanks to an automatic procedure, it is possible to balance backward and forward sweep limiting the growth of blade root torsional moments.
- Composite fibers misalignment F-BTC - fiber angles are varied in the laminates of spar caps and outer shell skin. Several setups prove capable of obtaining a good fatigue load reduction and a large room for trade-off is highlighted. The lower fatigue loads experienced by the F-BTC blades generate savings in the fatigue-driven tower design and room for a growth in rotor diameter.
- Offset in the positioning of spar caps and shear webs O-BTC - contrary to the studies performed on the very large offshore wind turbine rotors developed during recent European projects, here small or no benefits are obtained by offsetting spar caps and shear webs to obtain bend-twist coupling. The main cause is identified in the more pronounced blade slenderness, which limits the magnitude of allowable offsets.
- Regulation trajectory for BTC rotors - a traditional regulation trajectory designs a constant pitch angle strategy below rated conditions. This is sub-optimal for BTC rotors and a new regulation trajectory is developed where pitch and tip speed ratio are varied both below and above rated wind speed. Thanks to the change, the AEP losses typically generated by BTC rotors are relegated to marginal values at a cost of a slightly higher pitch actuator duty cycle.
- Soft BTC rotor - a final optimization exercise is run on a swept rotor equipped with twisted fibers in laminates of shell skin and spar caps. Thanks to the passive load alleviating technologies, a growth in rotor size at constant ultimate and fatigue loads is accomplished.  $C_p$ -Max automatically identifies a high-cone-angle low-natural-frequency rotor configuration as optimum, producing marked advantages in terms of masses, loads and ultimately a CoE reduction of 2.8%.

The field of wind turbine design is in a continuous evolution and several development activities are ongoing, especially on the methodological aspects. Here, high priority is assigned to four tasks. First, a load-based procedure to size the components between rotor and tower such as shaft, drive-train and generator is being implemented. This is expected to play an important role within an integrated design framework to more exactly evaluate couplings between rotor and system components. Secondly, modules to estimate the noise emissions of a wind turbine are being integrated within the design methodologies in order to include noise as a design criteria. Third, soft-coned-swept rotors approach the limits of applicability of the BEM formulation. Higher fidelity tools such as vortex methods are under development [?] and will be integrated within design methodologies. Finally, efforts are being dedicated to develop a probabilistic framework for the propagation of uncertainties that affect wind turbine simulation and design. This should ultimately lead to robust design methodologies.

## ACKNOWLEDGEMENTS

This work has greatly benefit from the activities of the IEA Wind Task 37 and the authours would like to thank the operating agents Katherine Dykes, Karl Merz, Frederik Zahle and Pierre-Elouan Réthoré for their great effort in coordinating the various studies.

## REFERENCES

1. Bottasso CL, Campagnolo F, Croce A. Multi-disciplinary constrained optimization of wind turbines. *Multibody Syst. Dyn.*, 2012;27(1):21-53. doi: [10.1007/s11044-011-9271-x](https://doi.org/10.1007/s11044-011-9271-x).
2. Bottasso CL, Bortolotti P, Croce A, Gualdoni, F. Integrated aero-structural optimization of wind turbine rotors. *Multibody Syst. Dyn.*, 2016;38(4):317-344. doi: [10.1007/s11044-015-9488-1](https://doi.org/10.1007/s11044-015-9488-1).
3. Bortolotti P, Bottasso CL, Croce A. Combined preliminary-detailed design of wind turbines. *Wind Energ. Sci.*, 2016;1(1):71-88. doi: [10.5194/wes-1-71-2016](https://doi.org/10.5194/wes-1-71-2016).
4. Dykes K, Ning SA, Graf P, et al. WISDEM 0.1.0 Documentation. 2017. <http://wisdem.github.io/WISDEM/>.
5. Zahle F, et al. HAWTOpt2 Documentation. 2017. <https://gitlab.windenergy.dtu.dk/HAWTOpt2>.
6. IEC 61400-1. Wind Turbines - Part 1: Design Requirements. Ed. 3., International Standard, International Electrotechnical Commission, 2005.
7. Sartori L, Bortolotti P, Croce A, Bottasso CL. Integration of prebend optimization in a holistic wind turbine design tool. *Journal of Physics, Conference Series*, 2016;753. doi: [10.1088/1742-6596/753/6/062006](https://doi.org/10.1088/1742-6596/753/6/062006).
8. Bortolotti P, Adolphs G, Bottasso CL. A methodology to guide the selection of composite materials in a wind turbine rotor blade design process. *Journal of Physics, Conference Series*, 2016;753. doi: [10.1088/1742-6596/753/6/062001](https://doi.org/10.1088/1742-6596/753/6/062001).

9. Dykes K, Rethore PE, Zahle F, Merz K. Wind Energy Systems Engineering: Integrated RD&D. IEA Task 37 Final Proposal, 2015. <https://sites.google.com/site/ieawindtask37/>.
10. MATLAB Documentation, 2017. [www.mathworks.com](http://www.mathworks.com).
11. Bottasso CL, Croce A, Savini B, Sirchi W, Trainelli L. Aero-servo-elastic modeling and control of wind turbines using finite-element multibody procedures. *Multibody Syst. Dyn.*, 2006;16(3):291-308. doi: [10.1007/s11044-006-9027-1](https://doi.org/10.1007/s11044-006-9027-1).
12. Giavotto V, Borri M, Mantegazza P, Ghiringhelli G. Anisotropic beam theory and applications. *Comput. Struct.*, 1983;16(1-4):403-413. doi: [10.1016/0045-7949\(83\)90179-7](https://doi.org/10.1016/0045-7949(83)90179-7).
13. Fingersh L, Hand M, Laxson A. Wind turbine design cost and scaling model. Technical Report NREL/TP-500-40566, 2006.
14. Chaviaropoulos PK, Sieros G. Design of Low Induction Rotors for use in large offshore wind farms. EWEA 2014 Conference, Barcelona, Spain, 2014.
15. Johans W, Griffith DT: Large Blade Manufacturing Cost Studies Using the Sandia Blade Manufacturing Cost Tool and Sandia 100-meter Blades. Sandia National Laboratories, Tech. Rep., 2013.
16. MSC NASTRAN 2012 Quick Reference Guide. MSC Software, 2012.
17. Bottasso CL, Campagnolo F, Croce A, Dilli S, Gualdoni F, Nielsen MB. Structural optimization of wind turbine rotor blades by multi-level sectional/multibody/3D-FEM analysis. *Multibody Syst. Dyn.*, 2014;32(1):87-116. doi: [10.1007/s11044-013-9394-3](https://doi.org/10.1007/s11044-013-9394-3).
18. Jonkman BJ, Kilcher L. TurbSim User's Guide: Version 1.06.00. NREL Technical Report, September, 2012.
19. XFOIL Documentation, <http://web.mit.edu/drela/Public/web/xfoil/>, 2017.
20. Guo Y, Parsons T, King R, Dykes K, Veers P. An Analytical Formulation for Sizing and Estimating the Dimensions and Weight of Wind Turbine Hub and Drivetrain Components, National Renewable Energy Laboratory, June 2015.
21. INNWIND.EU Design of state of the art 10-20MW offshore wind turbines. <http://www.innwind.eu/>.
22. UpWind, Integrated Wind Turbine Design. 2006-2011, [http://cordis.europa.eu/project/rcn/78583\\_en.html](http://cordis.europa.eu/project/rcn/78583_en.html).
23. AVATAR, Advanced Aerodynamic Tools for Large Rotors. <http://www.eera-avator.eu>.
24. Veers PS, Bir G, Lobitz DW. Aeroelastic tailoring in wind-turbine blade application. Windpower 98, AWEA Annual Conference and Exhibition, Bakersfield, CA, 27 April-May 1998.
25. Bottasso CL, Campagnolo F, Tibaldi C. Optimization-Based Study of Bend-Twist Coupled Rotor Blades for Passive and Integrated Passive/Active Load Alleviation. *Wind Energy*, 2013;16(8):1149-1166. doi: [10.1002/we.1543](https://doi.org/10.1002/we.1543).
26. Liebst BS. Wind turbine gust load alleviation utilizing curved blades. *Journal of Propulsion*, 1986;2(4):371-377. doi: [10.2514/3.22897](https://doi.org/10.2514/3.22897).
27. Zuteck M. Adaptive blade concept assessment: curved planform induced twist investigation. Sandia Report SAND 2002-2996, Sandia National Laboratories, Albuquerque, NM, October 2002.
28. Croce A, Sartori L, Lunghini MS, Clozza L, Bortolotti P, Bottasso CL. Lightweight Rotor Design by Optimal Spar Cap Offset. *Journal of Physics, Conference Series*, 2016;753. doi: [10.1088/17426596/753/6/062003](https://doi.org/10.1088/17426596/753/6/062003).
29. Sartori L, Bortolotti P, Lunghini MS, Croce A, Bottasso CL. On the effects of the integration of multiple load mitigation technologies on a 10 MW rotor. *Wind Energy Science*, Under Submission, 2017.